



Published in final edited form as:

Nature. 2011 January 13; 469(7329): 175–180. doi:10.1038/nature09648.

## Structure of a nanobody-stabilized active state of the $\beta_2$ adrenoceptor

Søren G. F. Rasmussen<sup>1,8,\*</sup>, Hee-Jung Choi<sup>1,2,\*</sup>, Juan Jose Fung<sup>1,\*</sup>, Els Pardon<sup>3,4</sup>, Paola Casarosa<sup>5</sup>, Pil Seok Chae<sup>6</sup>, Brian T. DeVree<sup>7</sup>, Daniel M. Rosenbaum<sup>1</sup>, Foon Sun Thian<sup>1</sup>, Tong Sun Kobilka<sup>1</sup>, Andreas Schnapp<sup>5</sup>, Ingo Konetzki<sup>5</sup>, Roger K. Sunahara<sup>7</sup>, Samuel H. Gellman<sup>6</sup>, Alexander Pautsch<sup>5</sup>, Jan Steyaert<sup>3,4</sup>, William I. Weis<sup>1,2,#</sup>, and Brian K. Kobilka<sup>1,#</sup>

<sup>1</sup> Department of Molecular and Cellular Physiology, Stanford University School of Medicine, 279 Campus Drive, Stanford, California 94305, USA

<sup>2</sup> Department of Structural Biology, Stanford University School of Medicine, 279 Campus Drive, Stanford, California 94305, USA

<sup>3</sup> Department of Molecular and Cellular Interactions, Vlaams Instituut voor Biotechnologie (VIB), Vrije Universiteit Brussel, B-1050 Brussels, Belgium

<sup>4</sup> Structural Biology Brussels, Vrije Universiteit Brussel, B-1050 Brussels, Belgium

<sup>5</sup> Boehringer Ingelheim Pharma GmbH & Co. KG, Germany

<sup>6</sup> Department of Chemistry, University of Wisconsin, Madison, Wisconsin 53706, USA

<sup>7</sup> Department of Pharmacology, University of Michigan Medical School, Ann Arbor MI, USA

<sup>8</sup> Department of Neuroscience and Pharmacology, The Panum Institute, University of Copenhagen, Blegdamsvej 3, 2200 Copenhagen N, Denmark

### Abstract

Users may view, print, copy, download and text and data- mine the content in such documents, for the purposes of academic research, subject always to the full Conditions of use: [http://www.nature.com/authors/editorial\\_policies/license.html#terms](http://www.nature.com/authors/editorial_policies/license.html#terms)

#Correspondence and requests for materials should be addressed to B.K.K. (kobilka@stanford.edu) or W.I.W (bill.weis@stanford.edu).

\*These authors contributed equally to this work.

Supplementary Information is linked to the online version of the paper at [www.nature.com/nature](http://www.nature.com/nature)

**Author Contributions** S.G.F.R. screened and characterized high affinity agonists, identified and determined dissociation rate of BI-167107, screened, identified and characterized MNG-3, performed selection and characterization of nanobodies, purified and crystallized the receptor with Nb80 in LCP, optimized crystallization conditions, grew crystals for data collection, reconstituted receptor in HDL particles and determined the effect of Nb80 and Gs on receptor conformation and ligand binding affinities, assisted with data collection and preparing the manuscript. H.J.C. managed data processing, solved and refined the structure, and assisted with preparing the manuscript. J.J.F. expressed, purified, selected and characterized nanobodies, purified and crystallized receptor with nanobodies in bicelles, assisted with growing crystals in LCP, and assisted with data collection. E.P. performed immunization, cloned and expressed nanobodies, and performed the initial selections. J.S. supervised nanobody production. P.S.K. and S.H.G. provided MNG-3 detergent for stabilization of purified  $\beta_2$ AR. B.D. and R.K.S. provided ApoA1 and Gs protein, and reconstituted  $\beta_2$ AR in HDL particles with Gs. D.R. characterized the usefulness of MNG-3 for crystallization in LCP and assisted with manuscript preparation. F.S.T. expressed  $\beta_2$ AR in insect cells and with T.S.K. performed the initial stage of  $\beta_2$ AR purification. A.P., A.S. assisted in selection of the high-affinity agonist BI-167,107. I.K. synthesized BI-167,107. P.C. characterized the functional properties of BI-167,107 in CHO cells. W.I.W. oversaw data processing, structure determination and refinement, and assisted with manuscript preparation. B.K.K. was responsible for the overall project strategy and management, prepared  $\beta_2$ AR in lipid vesicles for immunization, harvested and collected data on crystals, wrote the manuscript.

**Author Information** Reprints and permissions information is available at [www.nature.com/reprints](http://www.nature.com/reprints). Coordinates and structure factors for  $\beta_2$ AR-Nb80 are deposited in the Protein Data Bank (accession code 3POG).

G protein coupled receptors (GPCRs) exhibit a spectrum of functional behaviors in response to natural and synthetic ligands. Recent crystal structures provide insights into inactive states of several GPCRs. Efforts to obtain an agonist-bound active-state GPCR structure have proven difficult due to the inherent instability of this state in the absence of a G protein. We generated a camelid antibody fragment (nanobody) to the human  $\beta_2$  adrenergic receptor ( $\beta_2$ AR) that exhibits G protein-like behavior, and obtained an agonist-bound, active-state crystal structure of the receptor-nanobody complex. Comparison with the inactive  $\beta_2$ AR structure reveals subtle changes in the binding pocket; however, these small changes are associated with an 11 Å outward movement of the cytoplasmic end of transmembrane segment 6, and rearrangements of transmembrane segments 5 and 7 that are remarkably similar to those observed in opsin, an active form of rhodopsin. This structure provides insights into the process of agonist binding and activation.

## GPCR Active States

GPCRs activated by diffusible ligands exhibit a spectrum of functional states<sup>1</sup>. A GPCR may activate more than one G protein isoform or a G protein independent pathway such as arrestin. In the absence of a ligand, many GPCRs exhibit some basal, agonist independent activity towards one or more of these signaling pathways. Orthosteric ligands (compounds that occupy the native hormone binding pocket) are classified according to their efficacy, *i.e.*, the effect that they have on receptor signaling through a specific pathway. Inverse agonists inhibit basal activity while agonists maximally activate the receptor. Partial agonists induce submaximal activity, even at saturating concentrations. Neutral antagonists have no effect on basal activity, but sterically block the activity of other ligands. Moreover, the efficacy profile of ligands for a given GPCR can differ for different down-stream signaling pathways. The presence of some activity in the unliganded receptor implies low energy barriers between functional states, such that thermal fluctuations significantly sample activating conformations, and ligands with distinct efficacy profiles act by stabilizing distinct subsets of conformations.

We know little about the structural basis for the functional versatility of GPCRs. Only rhodopsin has been crystallized in different conformational states<sup>2,3,4,5</sup>. The first structures of rhodopsin covalently bound to 11-cis-retinal represent a completely inactive state with virtually no basal activity<sup>5</sup>. Structures of opsin, the ligand free form of rhodopsin, obtained from crystals grown at pH 5.6 likely represent active conformations<sup>2,3</sup>. The FTIR spectrum of opsin at acidic pH resembles that of metarhodopsin II, the light activated form of rhodopsin<sup>6</sup>. For rhodopsin, the light-induced transition from the inactive to the active state is very efficient. Rhodopsin is activated by photoisomerization of a covalent ligand, with efficient transfer of energy from the absorbed photon to the receptor. Crystal structures of low-pH opsin reveal that the protein conformation is the same in the presence or absence of a peptide from the alpha subunit of transducin (Gt), its cognate G protein, consistent with the notion that metarhodopsin II can adopt a fully active conformation in the absence of Gt.

The crystal structures of GPCRs activated by diffusible ligands, including the human  $\beta_2$ AR<sup>7,8,9,10</sup>, the avian  $\beta_1$ AR<sup>11</sup>, and the human adenosine A2A receptor<sup>12</sup>, represent inactive conformations bound by inverse agonists. Unlike the activation of rhodopsin by light, agonists are much less efficient at stabilizing the active state of the  $\beta_2$ AR, making it difficult

to capture this state in a crystal structure. Fluorescence lifetime studies show that even saturating concentrations of the full agonist isoproterenol do not stabilize a single active conformation<sup>13</sup>. This may be due to the relatively low affinity and rapid rates of association and dissociation for  $\beta_2$ AR agonists. Experiments using a  $\beta_2$ AR labeled with a conformationally sensitive fluorescent probe show that stabilization of the active state requires both agonist and Gs, the stimulatory G protein for adenylyl cyclase<sup>14</sup>. Efforts to obtain an agonist-GPCR-G protein complex are of great importance; however, this is a particularly difficult endeavor due to the biochemical challenges in working with both GPCRs and G proteins, and the inherent instability of the complex in detergent solutions. As an alternate approach, we developed a binding protein that preferentially binds to and stabilizes an active conformation, acting as a surrogate for Gs.

### Nanobody-stabilized $\beta_2$ AR active state

The active G protein coupled state of the  $\beta_2$ AR (and many other family A GPCRs) exhibits characteristic functional properties. Agonists promote Gs binding to the  $\beta_2$ AR and G protein binding to the receptor increases agonist affinity. We identified a camelid antibody fragment that exhibits G protein-like behavior towards the  $\beta_2$ AR. Tylopoda (camels, dromedaries and llamas) have developed a unique class of functional antibody molecules that are devoid of light chains<sup>15</sup>. A nanobody (Nb) is the recombinant minimal-sized intact antigen-binding domain of such a camelid heavy chain antibody and is approximately 25% the size of a conventional Fab fragment. To generate receptor specific nanobodies, a llama was immunized with purified agonist bound  $\beta_2$ AR reconstituted at high density into phospholipid vesicles. A library of single chain nanobody clones was generated and screened against agonist bound receptor. We identified seven clones that recognized agonist bound  $\beta_2$ AR. Of these, Nb80, was chosen because it exhibited G-protein-like properties upon binding to both wild type  $\beta_2$ AR and  $\beta_2$ AR-T4L, the  $\beta_2$ AR-T4 lysozyme fusion protein used to obtain the high-resolution inactive state crystal structure<sup>7,9</sup>.

We compared the effect of Nb80 with Gs on  $\beta_2$ AR structure and agonist binding affinity.  $\beta_2$ AR was labeled at the cytoplasmic end of TM6 at C265 with monobromobimane and reconstituted into HDL particles. TM6 moves relative to TM3 and TM5 upon agonist activation (Fig. 1A), and we have previously shown that the environment around bimane covalently linked to C265 changes with both agonist binding and G protein coupling, resulting in a decrease in bimane intensity and a red shift in  $\lambda_{\max}$ <sup>14</sup>. As shown in Fig. 1B, the catecholamine agonist isoproterenol and Gs both stabilize an active-like conformation, but the effect of Gs is greater in the presence of isoproterenol, consistent with the cooperative interactions of agonist and Gs on  $\beta_2$ AR structure. Nb80 alone has an effect on bimane fluorescence and  $\lambda_{\max}$  of unliganded  $\beta_2$ AR that is similar to that of Gs (Fig. 1C). This effect was not observed in  $\beta_2$ AR bound to the inverse agonist ICI-118,551. The effect of Nb80 was increased in the presence of 10  $\mu$ M isoproterenol. These results show that Nb80 does not recognize the inactive conformation of the  $\beta_2$ AR, but binds efficiently to agonist occupied  $\beta_2$ AR and produces a change in bimane fluorescence that is indistinguishable from that observed in the presence of Gs and isoproterenol.

Figure 1D and E shows the effect of Gs and Nb80 on agonist affinity for  $\beta_2$ AR.  $\beta_2$ AR was reconstituted into HDL particles and agonist competition binding experiments were performed in the absence or presence of Nb80 and Gs. In the absence of either protein, isoproterenol has an inhibition constant ( $K_i$ ) of 107 nM. In the presence of Gs two affinity states are observed, because not all of the  $\beta_2$ AR is coupled to Gs. In the Gs coupled state the affinity of isoproterenol increases by 100-fold ( $K_i = 1.07$  nM) (Fig 1D and Table S1). Similarly, in the presence of Nb80 the affinity of isoproterenol increases by 95-fold ( $K_i = 1.13$  nM) (Fig. 1E and Table S1). In contrast, Nb80 had little effect on  $\beta_2$ AR binding to the inverse agonist ICI-118,551 (Supplementary Figure 1 and Table S1). These binding data suggest that Nb80 stabilizes a conformation in WT  $\beta_2$ AR that is very similar to that stabilized by Gs, such that the energetic coupling of agonist and Gs binding is faithfully mimicked by Nb80.

The high-resolution structure of the inactive state of the  $\beta_2$ AR was obtained with a  $\beta_2$ AR-T4L fusion protein. We previously showed that  $\beta_2$ AR-T4L has a higher affinity for isoproterenol than WT  $\beta_2$ AR<sup>7</sup>. Nevertheless, in the presence of Nb80 the affinity increased by 60-fold, resulting in an affinity ( $K_i = 0.56$  nM) comparable to that of WT  $\beta_2$ AR bound to Nb80 (Fig 1F and Table S1). While we cannot study G protein coupling in  $\beta_2$ AR-T4L due to steric hindrance by T4L, the results show that T4L does not prevent binding of Nb80, and the nearly identical  $K_i$  values for agonist binding to wild-type  $\beta_2$ AR and  $\beta_2$ AR-T4L in the presence of Nb80 suggest that Nb80 stabilizes a similar conformation in these two proteins. The most likely explanation for the ability of Nb80 to bind to  $\beta_2$ AR-T4L while Gs does not is the difference in size of these two proteins. Nb80 is approximately 14 kDa while the Gs heterotrimer is approximately 90 kDa.

### High affinity $\beta_2$ AR agonist

To further stabilize the active state of the  $\beta_2$ AR, we screened over 50 commercial and proprietary  $\beta_2$ AR ligands. Of these, BI-167107 (Boehringer Ingelheim) had the most favorable efficacy, affinity and off-rate profile. BI-167107 is a full agonist that binds to the  $\beta_2$ AR with a dissociation constant  $K_d$  of 84 pM (Supplementary Figure 2A and B). As shown in Supplementary Fig 2C and D, BI-167107 induces a larger change in the fluorescence intensity and  $\lambda_{max}$  of bimane bound to C265 than does the agonist isoproterenol. Moreover, the rate of dissociation of BI-167107 was extremely slow. Displacement of BI-167107 with an excess of the neutral antagonist alprenolol required 150 hours to complete as compared with 5 sec for isoproterenol.

### Crystallization of $\beta_2$ AR-T4L-Nb80 complex

The  $\beta_2$ AR was originally crystallized bound to the inverse agonist carazolol using two different approaches. The first crystals were obtained from  $\beta_2$ AR bound to a Fab fragment that recognized an epitope composed of the amino and carboxyl terminal ends of the third intracellular loop connecting TMs 5 and 6<sup>8</sup>. In the second approach, the third intracellular loop was replaced by T4 lysozyme ( $\beta_2$ AR-T4L)<sup>7</sup>. Efforts to crystallize  $\beta_2$ AR-Fab complex and  $\beta_2$ AR-T4L bound to BI-167107 and other agonists failed to produce crystals of sufficient quality for structure determination. We therefore attempted to crystallize

BI-167107 bound to  $\beta_2$ AR and  $\beta_2$ AR-T4L in complex with Nb80. While crystals of both complexes were obtained in lipid bicelles and lipidic cubic phase (LCP), high-resolution diffraction was only obtained from crystals of  $\beta_2$ AR-T4L-Nb80 grown in LCP. These crystals grew at pH 8.0 in 39–44% PEG400, 100 mM Tris, 4 % DMSO, and 1% 1,2,3-heptanetriol.

A merged data set at 3.5 Å was obtained from 23 crystals (Supplementary Table S2). The structure was solved by molecular replacement using the structure of the carazolol-bound  $\beta_2$ AR and a nanobody as search models. Supplementary Figure 3A shows the packing of the  $\beta_2$ AR-T4L-Nb80 complex in the crystal lattice. The receptor has interactions with lattice neighbors in several directions, and is relatively well ordered (Supplementary Figure 3A), with readily interpretable electron density for most of the polypeptide. Nb80 binds to the cytoplasmic end of the  $\beta_2$ AR, with the third complementarity determining region (CDR) loop projecting into the core of the receptor (Figure 2A, and Supplementary Figure 4).

### Agonist-stabilized changes in the $\beta_2$ AR

Figure 2B–D compares the inactive  $\beta_2$ AR structure (from the carazolol bound  $\beta_2$ AR-T4L structure) with the agonist bound  $\beta_2$ AR component of the  $\beta_2$ AR-T4L-Nb80 complex. The largest differences are found at the cytoplasmic face of the receptor, with outward displacement of TM5 and TM6 and an inward movement of TM7 and TM3 in the  $\beta_2$ AR-T4L-Nb80 complex relative to the inactive structure. There are relatively small changes in the extracellular surface (Fig. 2C). The second intracellular loop (ICL2) between TM3 and TM4 adopts a two-turn alpha helix (Fig. 2D), similar to that observed in the turkey  $\beta_1$ AR structure<sup>11</sup>. The absence of this helix in the inactive  $\beta_2$ AR structure may reflect crystal lattice contacts involving ICL2.

Figure 2A and Supplementary Figure 4A–C show details of interaction of Nb80 with the cytoplasmic side of the  $\beta_2$ AR. An eight amino acid sequence of CDR 3 penetrates into a hydrophobic pocket formed by amino acids from TM segments 3, 5, 6 and 7. A four amino acid sequence of CDR1 provides additional stabilizing interactions with cytoplasmic ends of TM segments 5 and 6. CDR3 occupies a position similar to the carboxyl terminal peptide of transducin in opsin<sup>2</sup> (Supplementary Fig 4C,D). The majority of interactions between Nb80 and the  $\beta_2$ AR are mediated by hydrophobic contacts.

When comparing the agonist- and inverse agonist-bound structures, the largest change is observed in TM6, with an 11.4Å movement of the helix at Glu268<sup>6.30</sup> (part of the ionic lock) (superscripts in this form indicate Ballesteros–Weinstein numbering for conserved GPCR residues<sup>16</sup>) (Fig. 2D). This large change is effected by a small clockwise rotation of TM6 in the turn preceding the conserved Pro288<sup>6.50</sup>, enabled by the interrupted backbone hydrogen bonding at the proline and repacking of Phe282<sup>6.44</sup> (see below), which swings the helix outward.

The changes in agonist bound  $\beta_2$ AR-T4L-Nb80 relative to the inactive carazolol-bound  $\beta_2$ AR-T4L are remarkably similar to those observed between rhodopsin and opsin<sup>2,3</sup> (Fig. 2E). The salt bridge in the ionic lock between highly conserved Arg131<sup>3.50</sup> and Asp/Glu130<sup>3.49</sup> is broken. In opsin, Arg135<sup>3.50</sup> interacts with Tyr223<sup>5.58</sup> in TM5 and a backbone

carbonyl of the transducin peptide. Arg131<sup>3.50</sup> of  $\beta_2$ AR likewise interacts with a backbone carbonyl of CDR3 of Nb80. However, Nb80 precludes an interaction between Arg131<sup>3.50</sup> and Tyr219<sup>5.58</sup>, even though the tyrosine occupies a similar position in opsin and agonist bound  $\beta_2$ AR-T4L-Nb80. As in opsin, Tyr326<sup>7.53</sup> of the highly conserved NPxxY sequence moves into the space occupied by TM6 in the inactive state. In carazolol-bound  $\beta_2$ AR-T4L we observed a network of hydrogen bonding interactions involving highly conserved amino acids in TMs 1, 2, 6 and 7 and several water molecules<sup>7</sup>. While the resolution of the  $\beta_2$ AR-T4L-Nb80 structure is inadequate to detect waters, it is clear that the structural changes we observe would substantially alter this network.

In contrast to the relatively large changes observed in the cytoplasmic domains of  $\beta_2$ AR-T4L-Nb80, the changes in the agonist-binding pocket are fairly subtle. Figure 3 shows a comparison of the binding pockets of the inverse agonist and agonist bound structures. An omit map of the ligand-binding pocket is provided in Supplementary Figure 5. Many of the interactions between the agonist BI-167107 and the  $\beta_2$ AR are similar to those observed with the inverse agonist carazolol. The alkylamine and the  $\beta$ -OH of both ligands form polar interactions with Asp113<sup>3.32</sup> in TM3, and with Asn312<sup>7.39</sup> and Tyr316<sup>7.43</sup> in TM7. The agonist has a longer alkyl substituent on the amine, which ends with a phenyl ring that lies in a hydrophobic pocket formed by Trp109<sup>3.28</sup>, Phe193<sup>5.32</sup> and Ile309<sup>7.36</sup>.

The greatest difference between inactive and active structures in the ligand-binding site is an inward bulge of TM5 centered around Ser207<sup>5.46</sup>, whose C $\alpha$  position shifts by 2.1 Å (Fig. 4A). In addition, there are smaller inward movements of TM6 and TM7. The basal activity displayed by the  $\beta_2$ AR suggests that the protein structure surrounding the binding pocket is relatively dynamic in the absence of ligand, such that it samples active and inactive conformations. The presence of Pro211<sup>5.50</sup> in the following turn, which cannot form a hydrogen bond with the backbone at Ser207<sup>5.46</sup>, likely lowers the barrier to the transition between the conformations observed in the presence of carazolol and BI-167107. There are extensive interactions between the carbonyl oxygen, amine and hydroxyl groups on the heterocycle of BI-167107 and Ser203<sup>5.42</sup> and 207<sup>5.46</sup> in TM5, as well as Asn293<sup>6.55</sup> in TM6 and Tyr308<sup>7.35</sup> in TM7. In contrast, there is only one polar interaction between the nitrogen in the heterocycle of carazolol and Ser203<sup>5.42</sup>. Interactions of Ser203<sup>5.42</sup>, Ser204<sup>5.43</sup> and Ser207<sup>5.46</sup> with catecholamine hydroxyls have been proposed based on mutagenesis studies showing that these serines are important for agonist binding and activation<sup>17,18</sup>. While Ser204<sup>5.43</sup> does not interact directly with the ligand, it forms a hydrogen bond with Asn293<sup>6.55</sup> on TM6, which is in turn linked to Tyr308<sup>7.35</sup> of ECL3 (Fig. 3A). This tyrosine packs against Phe193<sup>5.32</sup> of ECL2, and both residues move to close off the ligand-binding site from the extracellular space.

Asn293<sup>6.55</sup> contributes to enantiomeric selectivity for catecholamine agonists<sup>19</sup>. The  $\beta$ -OH of BI-167107 does not interact with Asn293<sup>6.55</sup>, but forms hydrogen bonds with Asp113<sup>3.32</sup> and Asn312<sup>7.39</sup>, similar to what is observed for carazolol in the inactive structure. The chirality of the  $\beta$ -OH influences the spatial position of the aromatic ring system in  $\beta_2$ AR ligands, so the effect of Asn293<sup>6.55</sup> on  $\beta$ -OH enantiomeric selectivity may arise from its direct interaction with the aromatic ring system of the ligand, as well as its positioning of Ser204<sup>5.43</sup> and Tyr308<sup>7.35</sup>, which also interact with this portion of the ligand. However,

BI-167107 is not a catecholamine, and it is possible that the  $\beta$ -OH of catecholamine agonists, such as epinephrine and norepinephrine, has a direct interaction with Asn293<sup>6.55</sup>, since mutation of Asn293<sup>6.55</sup> has a stronger influence on the preference for the chirality of the  $\beta$ -OH of catecholamine agonists, compared with non-catechol agonists and antagonists<sup>19</sup>.

Trp<sup>6.48</sup> is highly conserved in Family A GPCRs, and it has been proposed that its rotameric state plays a role in GPCR activation (rotamer toggle switch)<sup>20</sup>. We observe no change in the side chain rotamer of Trp286<sup>6.48</sup> in TM6 (Fig. 4A), which lies near the base of the ligand-binding pocket, although its position shifts slightly in concert with rearrangements of nearby residues Ile121<sup>3.40</sup> and Phe282<sup>6.44</sup>. While there is spectroscopic evidence for changes in the environment of Trp<sup>6.48</sup> upon activation of rhodopsin<sup>21</sup>, a rotamer change is not observed in the crystal structures of rhodopsin and low-pH opsin. Moreover, recent mutagenesis experiments on the serotonin 5HT4 receptor demonstrate that Trp<sup>6.48</sup> is not required for activation of this receptor by serotonin<sup>22</sup>. These observations suggest that while changes in hydrophobic packing alter the conformation of the receptor in this region, changes in the Trp<sup>6.48</sup> rotamer do not occur as part of the activation mechanism.

It is interesting to speculate how the small changes around the agonist-binding pocket are coupled to much larger structural changes in the cytoplasmic regions of TMs 5, 6 and 7 that facilitate binding of Nb80 and Gs. A potential conformational link is shown in Figure 4. Agonist interactions with Ser 203<sup>5.42</sup> and 207<sup>5.46</sup> stabilize a receptor conformation that includes a 2.1 Å inward movement of TM5 at position 207<sup>5.46</sup> and 1.4 Å inward movement of the conserved Pro211<sup>5.50</sup> relative to the inactive, carazolol-bound structure. In the inactive state, the relative positions of TM5, TM3, TM6 and TM7 are stabilized by interactions between Pro211<sup>5.50</sup>, Ile121<sup>3.40</sup>, Phe282<sup>6.44</sup> and Asn318<sup>7.45</sup>. The position of Pro211<sup>5.50</sup> observed in the agonist structure is incompatible with this network of interactions, and Ile121<sup>3.40</sup> and Phe282<sup>6.44</sup> are repositioned, with a rotation of TM6 around Phe282<sup>6.44</sup> leading to an outward movement of the cytoplasmic end of TM6.

Although some of the structural changes observed in the cytoplasmic ends of transmembrane domains of the  $\beta_2$ AR-T4L-Nb80 complex arise from specific interactions with Nb80, the fact that Nb80 and Gs induce or stabilize similar structural changes in the  $\beta_2$ AR, as determined by fluorescence spectroscopy and by agonist binding affinity, suggests that Nb80 and Gs recognize similar agonist stabilized conformations. The observation that the transmembrane domains of rhodopsin and the  $\beta_2$ AR undergo similar structural changes upon activation provides further support that the agonist-bound  $\beta_2$ AR-T4L-Nb80 represents an active conformation and is consistent with a conserved mechanism of G protein activation.

However, the mechanism by which agonists induce or stabilize these conformational changes likely differs for different ligands and for different GPCRs. The conformational equilibria of rhodopsin and  $\beta_2$ AR differ, as shown by the fact that rhodopsin appears to adopt a fully active conformation in the absence of a G protein<sup>23</sup> whereas  $\beta_2$ AR cannot<sup>14</sup>. Thus, the energetics of activation and conformational sampling can differ among different GPCRs, which likely gives rise to the variety of ligand efficacies displayed by these

receptors. An agonist need only disrupt one key intramolecular interaction needed to stabilize the inactive state, as constitutive receptor activity can result from single mutations of amino acids from different regions of GPCRs<sup>24</sup>. Thus, disruption of these stabilizing interactions either by agonists or mutations lowers the energy barrier separating inactive and active states and increases the probability that a receptor can interact with a G protein.

## METHODS SUMMARY

### Crystallization

Preparation of  $\beta_2$ AR-T4L and Nb80 are described in Supplementary Methods. BI-167107 bound  $\beta_2$ AR-T4L and Nb80 preincubated in 1:1.2 molar ratio were mixed in monoolein containing 10% cholesterol in 1:1.5 protein to lipid ratio (w/w). Initial crystallization leads were identified and optimized in 24-well glass sandwich plates using 50 nL protein:lipid drops overlaid with 0.8  $\mu$ l precipitant solution in each well and sealed with a glass cover slip. Crystals for data collection were grown at 20° C in hanging-drop format using 0.8  $\mu$ l reservoir solution (36 to 44% PEG 400, 100 mM Tris pH 8.0, 4 % DMSO, 1 % 1,2,3-heptanetriol) diluted 2 to 4-fold in water. Crystals grew to full size, typically 40 x 5 x 5  $\mu$ m<sup>3</sup>, within 7 to 10 days. Crystals were flash frozen and stored in liquid nitrogen with reservoir solution as cryoprotectant. Diffraction data collection and processing, and structure solution and refinement are described in Supplementary Methods.

## METHODS (in supplemental information)

### Preparation of $\beta_2$ AR-T4L and nanobody-80 for crystallography

$\beta_2$ AR-T4L was expressed in Sf-9 insect cell cultures infected with  $\beta_2$ AR-T4L baculovirus, and solubilized according to previously described methods<sup>25</sup>. Functional protein was obtained by M1 FLAG affinity chromatography (Sigma) prior to and following alprenolol-Sepharose chromatography<sup>25</sup>. In the second M1 chromatography step, receptor-bound alprenolol was exchanged for high affinity agonist BI-167107 and dodecylmaltoside was exchanged for the MNG-3 amphiphile (11,11-Bis- $\beta$ -D-maltopyranosidylmethyl-heneicosane, Supplementary Figure 6, obtained from Chae and Gellman, University of Wisconsin, Madison) for increased receptor stability. The agonist-bound and detergent-exchanged  $\beta_2$ AR-T4L was eluted in 10 mM HEPES pH 7.5, 100 mM NaCl, 0.02% MNG-3, and 10  $\mu$ M BI-167107 followed by removal of N-linked glycosylation by treatment with PNGaseF (NEB). The protein was concentrated to ~50 mg/ml with a 100 kDa molecular weight cut off Vivaspin concentrator (Vivascience).

Nanobody-80 (Nb80) bearing a C-terminal His<sub>6</sub> tag was expressed in the periplasm of *E. coli* strain WK6 following induction with IPTG. Cultures of 0.6 L were grown to OD<sub>600</sub> = 0.7 at 37°C in TB media containing 0.1% glucose, 2 mM MgCl<sub>2</sub>, and 50  $\mu$ g/ml ampicillin. Induced cultures were grown overnight at 28°C. Cells were harvested by centrifugation and lysed in ice-cold buffer (50 mM Tris pH 8.0, 12.5 mM EDTA, and 0.125 M sucrose), then centrifuged to remove cell debris. Nb80 was purified by nickel affinity chromatography, dialysed against buffer (10 mM HEPES pH 7.5, 100 mM NaCl), and spin concentrated to ~120 mg/ml.



## Crystallization

BI-167107 bound  $\beta_2$ AR-T4L and Nb80 were mixed in 1:1.2 molar ratio, incubated 2 hours at RT before mixing with liquefied monoolein (M7765, Sigma) containing 10% cholesterol (C8667, Sigma) in 1:1.5 protein to lipid ratio (w/w) using the twin-syringe mixing method developed by Martin Caffrey<sup>26</sup>. Initial crystallization leads were identified using in-house screens and optimized in 24-well glass sandwich plates using 50 nL protein:lipid drops manually delivered and overlaid with 0.8  $\mu$ l precipitant solution in each well and sealed with a glass cover slip. Crystals for data collection were grown at 20°C by hanging drop vapor diffusion using 0.8  $\mu$ l reservoir solution (36 to 44% PEG 400, 100 mM Tris pH 8.0, 4 % DMSO, 1 % 1,2,3-heptanetriol) diluted 2 to 4-fold in Milli-Q water. Crystals grew to full size within 7 to 10 days. Crystals were flash frozen and stored in liquid nitrogen with reservoir solution as cryoprotectant.

## Microcrystallography data collection and processing

Diffraction data were measured at beamline 23-ID of the Advanced Photon Source, using a 10  $\mu$ m diameter beam. Low dose 1.0° rotation images were used to locate and center crystals for data collection. Data were measured in 1.0° frames with exposure times typically 5–10 sec with a 5x attenuated beam. Only 5–10° of data could be measured before significant radiation damage occurred. Data were integrated and scaled with the HKL2000 package<sup>27</sup>.

## Structure solution and refinement

Molecular replacement phases were obtained with the program Phaser<sup>28</sup>. The search models were 1) the high-resolution carazolol-bound  $\beta_2$ AR structure, PDB id 2RH1, but with T4L and all water, ligand and lipid molecules removed) and a nanobody (PDB id 3DWT, water molecules removed) as search models. The rotation and translation function Z scores were 8.7 and 9.0 after placing the  $\beta_2$ AR model, and the nanobody model placed subsequently had rotation and translation function Z scores of 3.5 and 11.5. The model was refined in Phenix<sup>29</sup> and Buster<sup>30</sup>, using a group B factor model with one B for main chain and one B for side chain atoms. Refinement statistics are given in Table S2. Despite the strong anisotropy (Table S2), the electron density was clear for the placement of side chains.

## Ligand binding on receptor reconstituted in HDL particles

The effect of Nb80 and Gs on the receptors affinity for agonists was compared in competition binding experiments. The  $\beta_2$ AR and  $\beta_2$ AR-T4L (both truncated at position 365) purified as previously described<sup>7,8</sup> were reconstituted in high-density lipoprotein (HDL) particles followed by reconstitution of Gs into HDL particles containing  $\beta_2$ AR according to previously published methods<sup>31</sup>. 0.6 nM [<sup>3</sup>H]-dihydroalprenolol ([<sup>3</sup>H]-DHA) was used as radioligand and agonist (–)-isoproterenol (ISO) or inverse agonist ICI-118,551 (ICI) as competitor. Nb80 was used at 1  $\mu$ M. GTP $\gamma$ S was used at 10  $\mu$ M. TBS (50 mM Tris pH 7.4, 150 mM NaCl) containing 0.1% BSA was used as binding buffer. Bound <sup>3</sup>H-DHA was separated from unbound on a Brandel harvester by passing over a Whatman GF/B filter (presoaked in TBS with 0.3% polyethylenimine) and washed in cold TBS. Radioligand binding was measured in a Beckman LS6000 scintillation counter. Ligand binding affinity ( $K_d$ ) of DHA was determined from saturation binding curves using GraphPad Prism

software. Normalized ISO competition binding data were fit to a two-site competition binding model by using GraphPad Prism. Binding affinities of ISO ( $K_i$  values, tabulated in Table S1) were determined from  $IC_{50}$  values using the equation  $K_i = IC_{50} / (1 + [L] / K_d)$ .

### cAMP Assay

To determine the functional potency of BI-167107, changes in intracellular cAMP levels were determined with CHO-h $\beta_2$ AR cells in suspension (15,000 cells/well) by using Alphascreen technology (PerkinElmer Life and Analytical Sciences) and a 384-well plate format (Optiplate; PerkinElmer Life and Analytical Sciences), according to the manufacturer's protocol. In brief, cells were stimulated with the respective agonists at different concentrations in Hanks' buffered saline solution supplemented with 5 mM HEPES, 0.1% bovine serum albumin, and 500 mM 3-isobutyl-1-methylxanthine for 30 min at room temperature. Cells were lysed by using Alphascreen reagents. After 2 h, plates were read on an Envision plate reader (PerkinElmer Life and Analytical Sciences). The concentration of cAMP in the samples was calculated from a standard curve.

### Bimane fluorescence spectroscopy on $\beta_2$ AR reconstituted in HDL particles

To compare the effects on receptor conformation of Gs and Nb80 binding the purified  $\beta_2$ AR was labeled with the environmentally sensitive fluorescent probe monobromo-bimane (Invitrogen) at cysteine 265 located in the cytoplasmic end of TM6, and reconstituted into HDL particles (mBB- $\beta_2$ AR/HDL). Prior to obtaining fluorescence emission spectra, 10 nM mBB- $\beta_2$ AR/HDL was incubated 30 min at RT in buffer (20 mM HEPES pH 7.5, 100 mM NaCl) in the absence or presence of 10  $\mu$ M ISO, 1  $\mu$ M ICI, 300 nM Gs heterotrimer, or 300 nM Nb80, or in combinations of ISO with Gs, ISO with Nb80, and ICI with Nb80. Fluorescence spectroscopy was performed on a Spex FluoroMax-3 spectrofluorometer (Jobin Yvon Inc.) with photon-counting mode, using an excitation and emission bandpass of 5 nm. Excitation was set at 370 nm and emission was collected from 415 to 535 nm in 1 nm increments with 0.3 sec/nm integration time. Fluorescence intensity was corrected for background fluorescence from buffer and ligands. The curves shown in Figure 1B and 1C are each the average of triplicate experiments.

### High affinity $\beta_2$ AR agonist screening by bimane fluorescence spectroscopy

To obtain high affinity agonist candidates with slow dissociation rates for crystallography, a screening process of commercially available drugs and compound libraries from medicinal and biotech industry was initiated. Screening was conducted in several rounds on more than 50 compounds. 10  $\mu$ M of each compound incubated with 100 nM purified mBB- $\beta_2$ AR in DDM buffer (20 mM HEPES pH 7.5, 100 mM NaCl, 0.1% dodecylmaltoside (DDM)) for 30 min at RT prior to emission scanning, using same equipment and settings as described in the section above. Compounds inducing the largest red shift in  $\lambda_{max}$  and decrease in bimane fluorescence emission were identified. Closely related structural analogs were subsequently screened using same criteria for selection. Several lead candidate compounds were then subjected to dissociation experiments to identify the agonist with the slowest rate of dissociation. In these experiments, 100 nM mBB- $\beta_2$ AR was incubated with 1  $\mu$ M lead compound in DDM buffer for 2 hours at RT before obtaining the emission scan at  $t=0$

(example in figure 2D, green spectra). An excess amount (200  $\mu\text{M}$ ) of the neutral antagonist alprenolol (ALP) was added to identical samples followed by measurement of bimeane emission at various time points in a period up to 7 days or until complete dissociation of agonist.

## Supplementary Material

Refer to Web version on PubMed Central for supplementary material.

## Acknowledgments

We acknowledge support from National Institutes of Health Grants NS028471 and GM083118, and GM56169 (W.I.W.), a grant from Boehringer Ingelheim (B.K.K.), the Mathers Foundation (B.K.K and W.I.W), the Lundbeck Foundation (Junior Group Leader Fellowship, S.G.F.R.), the Fund for Scientific Research of Flanders (FWO-Vlaanderen) and the Institute for the encouragement of Scientific Research and Innovation of Brussels (ISRIB) (E.P. and J.S.).

## References

1. Rosenbaum DM, Rasmussen SG, Kobilka BK. The structure and function of G-protein-coupled receptors. *Nature*. 2009; 459:356–363. [PubMed: 19458711]
2. Scheerer P, et al. Crystal structure of opsin in its G-protein-interacting conformation. *Nature*. 2008; 455:497–502. [PubMed: 18818650]
3. Park JH, Scheerer P, Hofmann KP, Choe HW, Ernst OP. Crystal structure of the ligand-free G-protein-coupled receptor opsin. *Nature*. 2008; 454:183–U133. [PubMed: 18563085]
4. Li J, Edwards PC, Burghammer M, Villa C, Schertler GF. Structure of bovine rhodopsin in a trigonal crystal form. *J Mol Biol*. 2004; 343:1409–1438. [PubMed: 15491621]
5. Palczewski K, et al. Crystal structure of rhodopsin: A G protein-coupled receptor. *Science*. 2000; 289:739–745. [PubMed: 10926528]
6. Vogel R, Siebert F. Conformations of the active and inactive states of opsin. *Journal of Biological Chemistry*. 2001; 276:38487–38493. [PubMed: 11502747]
7. Rosenbaum DM, et al. GPCR engineering yields high-resolution structural insights into beta2-adrenergic receptor function. *Science*. 2007; 318:1266–1273. [PubMed: 17962519]
8. Rasmussen SG, et al. Crystal structure of the human beta2 adrenergic G-protein-coupled receptor. *Nature*. 2007; 450:383–387. [PubMed: 17952055]
9. Cherezov V, et al. High-resolution crystal structure of an engineered human beta2-adrenergic G protein-coupled receptor. *Science*. 2007; 318:1258–1265. [PubMed: 17962520]
10. Hanson MA, et al. A specific cholesterol binding site is established by the 2.8 angstrom structure of the human beta(2)-adrenergic receptor. *Structure*. 2008; 16:897–905. [PubMed: 18547522]
11. Warne T, et al. Structure of a beta1-adrenergic G-protein-coupled receptor. *Nature*. 2008; 454:486–491. [PubMed: 18594507]
12. Jaakola VP, et al. The 2.6 Angstrom Crystal Structure of a Human A2A Adenosine Receptor Bound to an Antagonist. *Science*. 2008
13. Ghanouni P, et al. Functionally different agonists induce distinct conformations in the G protein coupling domain of the beta 2 adrenergic receptor. *J Biol Chem*. 2001; 276:24433–24436. [PubMed: 11320077]
14. Yao XJ, et al. The effect of ligand efficacy on the formation and stability of a GPCR-G protein complex. *Proc Natl Acad Sci U S A*. 2009; 106:9501–9506. [PubMed: 19470481]
15. Hamers-Casterman C, et al. Naturally occurring antibodies devoid of light chains. *Nature*. 1993; 363:446–448. [PubMed: 8502296]
16. Ballesteros JA, Weinstein H. Integrated methods for the construction of three-dimensional models and computational probing of structure-function relations in G protein coupled receptors. *Meth Neurosci*. 1995; 25:366–428.

17. Strader CD, et al. Identification of residues required for ligand binding to the  $\beta$ -adrenergic receptor. *Proc Natl Acad Sci U S A*. 1987; 84:4384–4388. [PubMed: 2885836]
18. Liapakis G, et al. The forgotten serine. A critical role for Ser-2035.42 in ligands binding to and activation of the beta 2-adrenergic receptor. *J Biol Chem*. 2000; 275:37779–37788. [PubMed: 10964911]
19. Wieland K, Zuurmond HM, Krasel C, Ijzerman AP, Lohse MJ. Involvement of Asn-293 in stereospecific agonist recognition and in activation of the beta 2-adrenergic receptor. *Proc Natl Acad Sci U S A*. 1996; 93:9276–9281. [PubMed: 8799191]
20. Shi L, et al. Beta2 adrenergic receptor activation. Modulation of the proline kink in transmembrane 6 by a rotamer toggle switch. *J Biol Chem*. 2002; 277:40989–40996. [PubMed: 12167654]
21. Ahuja S, Smith SO. Multiple switches in G protein-coupled receptor activation. *Trends Pharmacol Sci*. 2009; 30:494–502. [PubMed: 19732972]
22. Pellissier LP, et al. Conformational toggle switches implicated in basal constitutive and agonist-induced activated states of 5-hydroxytryptamine-4 receptors. *Mol Pharmacol*. 2009; 75:982–990. [PubMed: 19168624]
23. Altenbach C, Kusnetzow AK, Ernst OP, Hofmann KP, Hubbell WL. High-resolution distance mapping in rhodopsin reveals the pattern of helix movement due to activation. *Proc Natl Acad Sci U S A*. 2008; 105:7439–7444. [PubMed: 18490656]
24. Parnot C, Miserey-Lenkei S, Bardin S, Corvol P, Clauser E. Lessons from constitutively active mutants of G protein-coupled receptors. *Trends Endocrinol Metab*. 2002; 13:336–343. [PubMed: 12217490]
25. Kobilka BK. Amino and carboxyl terminal modifications to facilitate the production and purification of a G protein-coupled receptor. *Anal Biochem*. 1995; 231:269–271. [PubMed: 8678314]
26. Caffrey M, Cherezov V. Crystallizing membrane proteins using lipidic mesophases. *Nat Protoc*. 2009; 4:706–731. [PubMed: 19390528]
27. Otwinowski Z, Minor W. Processing of x-ray diffraction data collected in oscillation mode. *Methods Enzymol*. 1997; 276:307–326.
28. McCoy AJ, et al. Phaser crystallographic software. *J Appl Crystallogr*. 2007; 40:658–674. [PubMed: 19461840]
29. Afonine PV, Grosse-Kunstleve RW, Adams PD. A robust bulk-solvent correction and anisotropic scaling procedure. *Acta Crystallogr D Biol Crystallogr*. 2005; 61:850–855. [PubMed: 15983406]
30. Blanc E, et al. Refinement of severely incomplete structures with maximum likelihood in BUSTER-TNT. *Acta Crystallogr D Biol Crystallogr*. 2004; 60:2210–2221. [PubMed: 15572774]
31. Whorton MR, et al. A monomeric G protein-coupled receptor isolated in a high-density lipoprotein particle efficiently activates its G protein. *Proc Natl Acad Sci U S A*. 2007; 104:7682–7687. [PubMed: 17452637]
32. Zhang XJ, Wozniak JA, Matthews BW. Protein flexibility and adaptability seen in 25 crystal forms of T4 lysozyme. *J Mol Biol*. 1995; 250:527–552. [PubMed: 7616572]

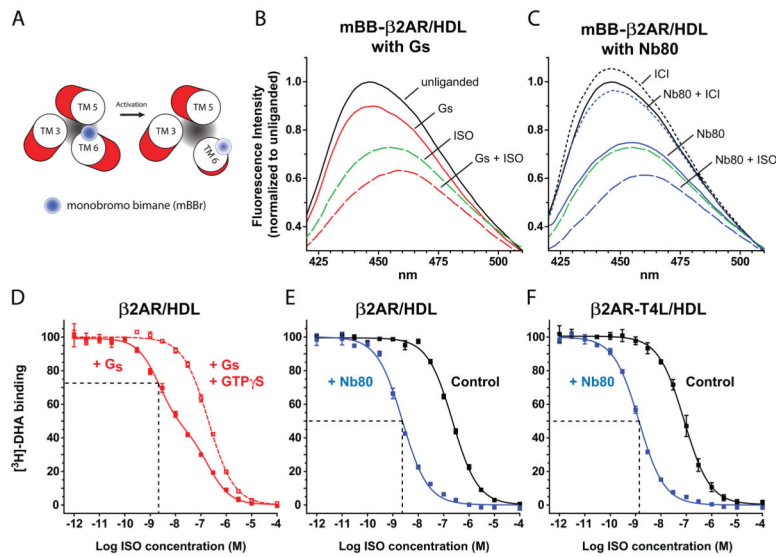


**Figure 1. Effect of Nb80 on β<sub>2</sub>AR structure and function**

**a**, The cartoon illustrates the movement of the environmentally-sensitive bimane probe attached to Cys265<sup>6,27</sup> in the cytoplasmic end of TM6 from a more buried, hydrophobic environment to a more polar, solvent-exposed position during receptor activation that results in a decrease in the observed fluorescence in Figure 1b–c and Supplementary Figure 2c–d. **b–c**, Fluorescence emission spectra showing ligand-induced conformational changes of monobromobimane labeled β<sub>2</sub>AR reconstituted into high density lipoprotein particles (mBB-β<sub>2</sub>AR/HDL) in the absence (black solid line) or presence of full agonist isoproterenol (ISO, green wide dashed line), inverse agonist ICI-118,551 (ICI, black dashed line), G<sub>s</sub> heterotrimer (red solid line), nanobody-80 (Nb80, blue solid lines), and combinations of G<sub>s</sub> with ISO (red wide dashed line), Nb80 with ISO (blue wide dashed line), and Nb80 with ICI (blue dashed line). **d–f** Ligand binding curves for ISO competing against [<sup>3</sup>H]-dihydroalprenolol ([<sup>3</sup>H]-DHA) for **d**, β<sub>2</sub>AR/HDL reconstituted with G<sub>s</sub> heterotrimer in the absence or presence of GTPγS, **e**, β<sub>2</sub>AR/HDL in the absence and presence of Nb80, and **f**, β<sub>2</sub>AR-T4L/HDL in the absence and presence of Nb80. Error bars represent standard errors.

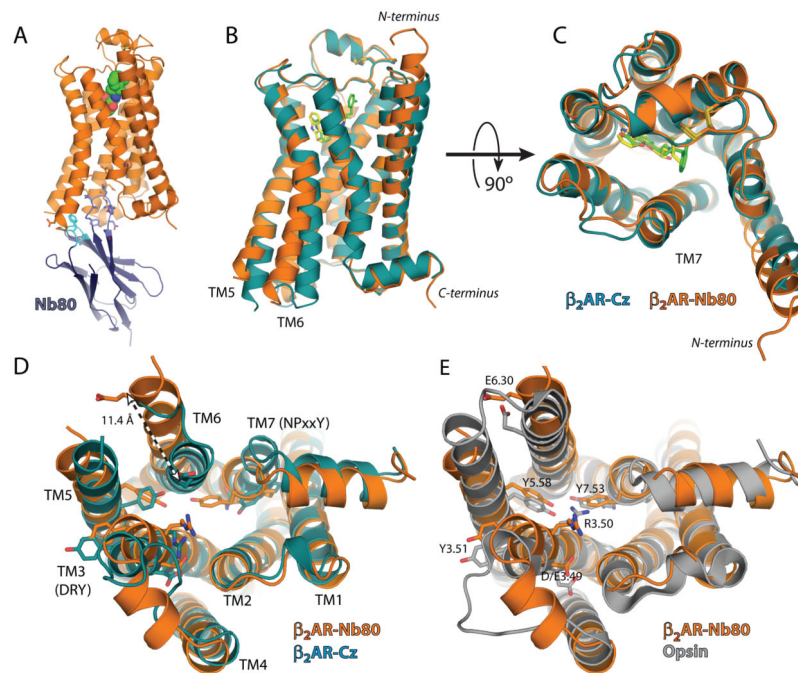


**Figure 2. Comparison of the agonist-Nb80 stabilized crystal structures of the  $\beta_2$ AR with inverse agonist bound  $\beta_2$ AR and opsin**

The structure of inverse agonist carazolol bound  $\beta_2$ AR-T4L ( $\beta_2$ AR-Cz) is shown in blue with the carazolol in yellow. The structure of BI-167107 agonist bound and Nb80 stabilized  $\beta_2$ AR-T4L ( $\beta_2$ AR-Nb80) is shown in orange with BI-167107 in green. These two structures were aligned using Pymol align function. **a**, Side view of the  $\beta_2$ AR-Nb80 complex with  $\beta_2$ AR in orange and CDRs of Nb80 in light blue (CDR1) and blue (CDR3). **b**, Side view of the superimposed structures showing significant structural changes in the intracellular and G protein facing part of the receptors. **c**, Comparison of the extracellular ligand binding domains showing modest structural changes. **d**, Cytoplasmic view showing the ionic lock interaction between Asp3.49 and Arg3.50 of the DRY motif in TM3 is broken in the  $\beta_2$ AR-Nb80 structure. The intracellular end of TM6 is moved outward and away from the core of the receptor. The intracellular end of TM6 is moved outward and away from the core of the receptor. The arrow indicates a 11.4 Å change in distance between the  $\alpha$ -carbon of Glu6.30 in the structures of  $\beta_2$ AR-Cz and  $\beta_2$ AR-Nb80. The intracellular ends of TM3 and TM7 move towards the core by 4 and 2.5 Å respectively, while TM5 moves outward by 6Å. **e**, The  $\beta_2$ AR-Nb80 structure superimposed with the structure of opsin crystallized with the C-terminal peptide of  $G_t$  (transducin) <sup>2</sup>. PyMOL (<http://www.pymol.org>) was used for the preparation of all structure figures.

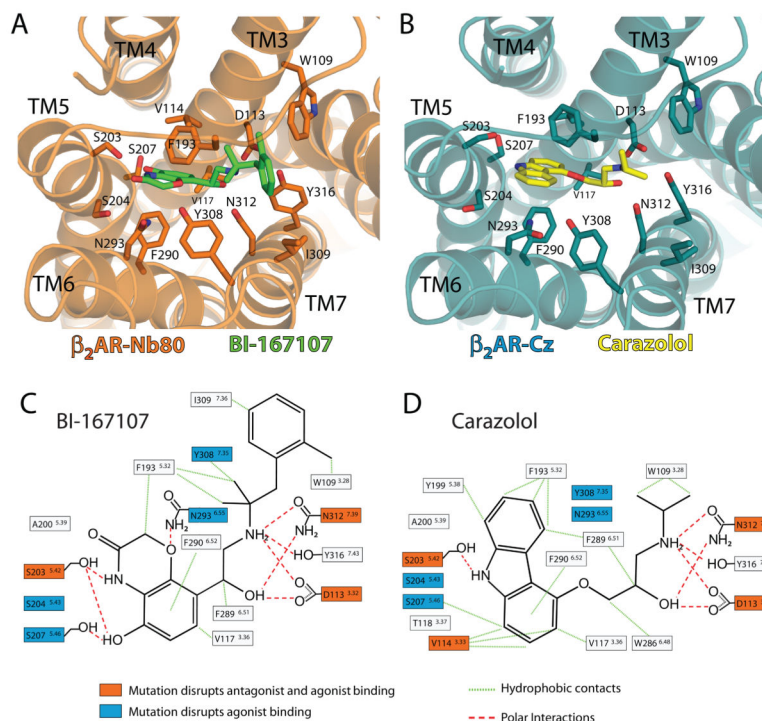


**Figure 3. Ligand binding pocket of BI-167107 and carazolol bound  $\beta_2$ AR structures**

Panels **a** and **b** depict extracellular views of the agonist BI-167107 and carazolol bound structures, respectively. Residues within 4Å of one or both ligands are shown as sticks. In all panels, oxygens are red and nitrogens are blue. Panels **c** and **d** show a schematic representation of the interactions between the  $\beta_2$ AR and the ligands BI-167107 and carazolol. The residues shown here have at least one atom within 4 Å of the ligand in the crystal structures. Mutations of amino acids in orange boxes have been shown to disrupt both antagonist and agonist binding. Mutations of amino acids in blue boxes have been shown to disrupt agonist binding. Green lines indicate potential hydrophobic interactions and orange lines indicate potential polar interactions.

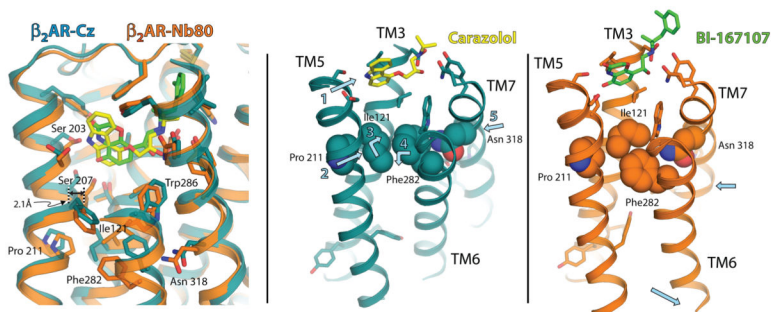


**Figure 4. Rearrangement of transmembrane segment packing interactions upon agonist binding**  
**a**, The BI-167107 and carazolol bound structures are superimposed to show structural differences propagating from the ligand binding pocket. BI-167107 and carazolol are shown with green and yellow bonds, respectively. **b**, Packing interactions that stabilize the inactive state are observed between Pro211 in TM5, Ile121 in TM3, Phe282 in TM6 and Asn318 in TM7. **c**, The inward movement of TM5 upon agonist binding disrupts the packing of Ile121 and Pro211 resulting in a rearrangement of interactions between Ile121 and Phe282. These changes contribute to a rotation and outward movement of TM6 and an inward movement of TM7.